KINETIC CHARACTERIZATION OF PLASMA SHEET DYNAMICS

G. K. PARKS, L. J. CHEN, M. FILLINGIM and M. MCCARTHY
Geophysics Program, Box 351650, University of Washington Seattle, WA 98195, U.S.A.

Abstract. The Wind spacecraft made 26 perigee passes through the near-earth plasma sheet region during 1994 to 1997. Nearly all of these passes obtained plasma data from substorms and bursty bulk flow (BBF) events. New features of ion distributions have been observed in both the plasma sheet boundary layer (PSBL) and the central plasma sheet (CPS) in the vicinity of the current sheet that are relevant for understanding the structure of the PSBL and the mechanisms of particle acceleration to MeV energies associated with the BBF events. Kinetic processes are key to understanding these new observations that are not adequately explained by existing magnetohydrodynamics (MHD) models and theories. This article will feature the phase space distribution functions as the primary data product. The main purpose of this article is to establish an observational framework for new improved models and theories. The new observations should challenge modelers and theorists.

1. Introduction

The geomagnetic tail plasma is rarely in equilibrium and the spectacular auroral displays are visual manifestations of the unstable dynamics. The challenge to long-standing unsolved space physics problems in the geomagnetic tail is to shed new light on the relationships of the dynamics occurring in the plasma sheet and the aurora. It has been known for over twenty years that dynamical activities occurring in the plasma sheet boundary layer (PSBL) and the central plasma sheet (CPS) are connected to the auroral processes. Great efforts have been made to understand them and the current knowledge of tail dynamics comes mainly from studying the bulk plasma moments. This approach reduces the 6N (N is the total number of particles) variables of a plasma distribution into three mean quantities, density, mean velocity and mean square velocity. The assumption is then made that the plasma is in equilibrium and consists of a single component. This permits the mean velocity to be interpreted as flow in the fluid sense and the mean square velocity as the temperature in the thermodynamic sense. This magnetohydrodynamic (MHD) approach has provided a useful picture. However, it is becoming increasingly evident that the neglect of kinetic processes is resulting in a less than accurate picture of the real plasma dynamics.

We have thus begun studying the plasma behavior in the plasma sheet using the distribution function as the primary data product. This approach has yielded new information on the plasma dynamics not revealed in the MHD fluid approach. This article will review several new discoveries that we have made recently about the

Space Science Reviews **95:** 237–255, 2001.
© 2001 *Kluwer Academic Publishers. Printed in the Netherlands.*

plasma behavior in the near-earth plasma sheet that have important implications about substorms. We will emphasize features revealed by kinetic distribution functions. Plasma moments are computed so that the new observations can be compared to previous studies that used bulk plasma parameters.

One of the most compelling science issue in the PSBL region concerns the sources of the field-aligned ion beams and what role they play in substorm dynamics. Previous observations showed unidirectional beams streaming only in the earthward direction in the outer-most region of the PSBL (Forbes *et al.*, 1982; Takahashi and Hones, 1988). New observations now show there is also a unidirectional beam streaming in the tailward direction just inside the earthward streaming beam (Parks *et al.*, 1998). This beam was missed by previous observations. The neutral line model predicts unidirectional earthward streaming and bidirectional beams but not the unidirectional tailward streaming beams. The problem now is to identify the source of this tailward streaming beam and the role it plays in the geomagnetic tail dynamics.

Another science issue concerns the high speed flows that are reported to be occurring only in the earthward direction (Baumjohann *et al.*, 1990). These flows in the PSBL come from ion beams and they are field-aligned. Thus, observations of only earthward flows are not consistent with the existence of tailward streaming beams that are as intense as the earthward streaming beams. We will demonstrate that studying the plasma behavior using only velocity moments is not adequate. This inadequacy is clearly illustrated in the case of counter streaming beams with equal velocities which yields a zero mean flow and would indicate the plasma is inactive when in fact it is very dynamic. Plasma distributions supporting beams are unstable. Using only velocity moments has lead to an incorrect conclusion. It is fundamentally important to examine the parent distribution function from which moments are derived.

In the CPS region in the vicinity of the current sheet, the most dynamic events are the bursty bulk flow (BBF) events (Angelopoulos *et al.*, 1992). Previous reports indicated BBFs have high speed ($>$400 km s^{-1}) $\mathbf{E}\times\mathbf{B}$ flows in the earthward direction. Detailed distribution function studies now indicate the high velocity moments of BBFs are not due to a $\mathbf{E}\times\mathbf{B}$ flow but rather they are consequences of as yet unidentified complex microphysical processes that produce highly anisotropic distributions of energetic ions up to MeV energies in association with the tail current disruption. (Chen *et al.*, 2000a). Our observations show that temporal variations (B/t) are very important. Previous studies also indicated that BBFs occur with auroral expansion onsets in the ionosphere (Angelopolous *et al.*, 1997; Fairfield *et al.*, 1999). The new observations indicate that BBFs can occur throughout a substorm event, even during weak auroral pseudobreakup events (Fillingim *et al.*, 2000). The BBFs are accompanied by intensification of the auroral kilometric radiation (AKR) and rapid magnetic field fluctuations whose frequency can be comparable to the local ion cyclotron frequency. These very different phenomena occur from auroral altitudes to the distant plasma sheet region and they are tied to common

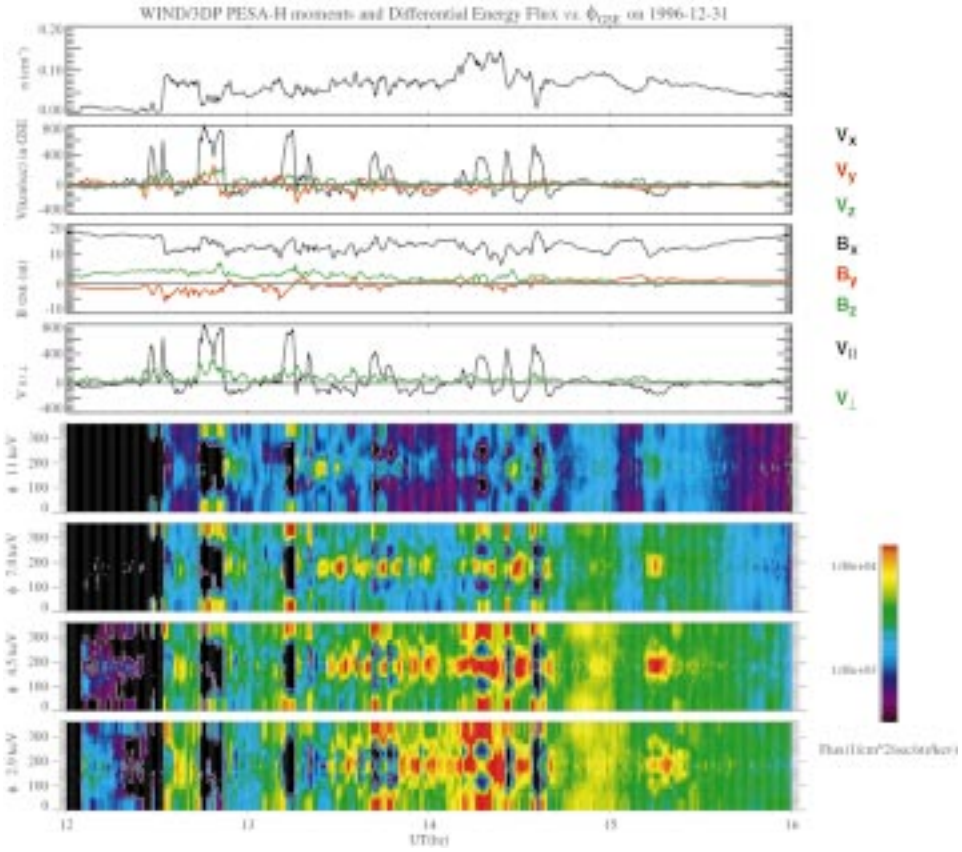

Figure 1. From top to bottom: ion density, ion velocity moments in GSE, magnetic field components, ion velocity parallel and perpendicular to the magnetic tield, and energy-angle spectrograms of elected ion energies. See text for detailed discussion.

but as yet unidentified processes that affect both global scale currents and kinetic particle distributions.

2. Dynamics in the PSBL

Figure 1 shows typical features of ion behavior in the PSBL (Ions are assumed to be protons in this aticle). The data come from the highly sensitive, large geometrical factor (1.6×10^{-2} cm^2 ster^{-1}) 3D electrostatic analyzers that detected ions with energies 70 eV to 28 keV (Lin *et al.*, 1995). The top two panels show the first two moments of the ion distribution function (density, mean velocity) obtained on December 31, 1996 when the Wind spacecraft passed through the near-earth plasma sheet. The moments are 24 s averages. The third panel shows the three components of the magnetic field (3 s averages) measured on Wind (courtesy of R.

Lepping) and the fourth panel shows the mean velocity, $\langle \mathbf{v} \rangle = \int \mathbf{v} f(\mathbf{r}, \mathbf{v}) d\mathbf{v}$, relative to the local magnetic field direction. The bottom four panels are energy-angle spectrograms. Here, the ordinate represents GSE Φ angles from 0-360° with 0° and 360° pointing in the sunward (earthward) direction and 180° in the antisunward (tailward) direction. The flux scale is shown on the right.

At 12:30 UT, as the plasma sheet expanded and engulfed the spacecraft, Wind crossed into the PSBL from the lobe. This resulted in the sharp increase of the density (0.1/cc). The low density (0.02/cc) plasma just outside the PSBL is due to the low energy plasma layer which is often present on the lobe side of PSBL (Parks *et al.*, 1992). The magnetic field **B** in the lobe was dominated by Bx. Inside the PSBL, it was smaller but still dominant. At 12:30 UT, the GSE position of Wind was (23.8, −3, 3), in earth radius (R_E) and the UVI images from Polar indicated that the aurora was fading in the ionosphere and the substorm was in the recovery phase (Figure 2).

DEPENDENCE OF VELOCITY MOMENTS ON THE DISTRIBUTION FUNCTION

The plasma behavior is often studied using velocity moments, $\langle \mathbf{v} \rangle$, and we now examine what kind of plasma distributions yield large $\langle \mathbf{v} \rangle$ values. Let us examine the second and the fourth panels that show large $\langle \mathbf{v} \rangle$ values during the two hours, 1230-1430 UT. Individual $\langle \mathbf{v} \rangle$ events typically lasted for 10 minutes and their values varied from a few hundred km s^{-1} to 800 km s^{-1}. The large $\langle \mathbf{v} \rangle$ values are mainly directed in the earthward direction ($+x$) and parallel to **B**. The values in the tailward direction ($-x$) are much smaller, 150 km s^{-1}. In the direction perpendicular to **B**, $\langle \mathbf{v}_\perp \rangle$ were $<$100 km s^{-1} except for the short period 12:48 UT when it reached 200 km s^{-1} in both y- and z-directions.

Comparison to the energy-angle plots shows that large $\langle \mathbf{v} \rangle$ values come from ion beams. For example, the high $\langle \mathbf{v} \rangle$ at 12:32 UT is associated with the unidirectional earthward streaming (0 and 360°) ion beam at the edge of the PSBL. When the spacecraft approached the PSBL edge again at 12:44 UT, the earthward streaming beam was once again detected and high $\langle \mathbf{v} \rangle$ values accompanied. The ion beams (also unidirectional) streaming in the tailward direction (180°) yield much smaller $\langle \mathbf{v} \rangle$ even though the tailward streaming beams are as intense as the earthward going beams (see the beam just inside the earthward streaming beam at 12:32 UT). To shed light on why this is so, note first the contrasting features that surround the earthward and tailward streaming beams in the energy-angle plots. When earthward streaming beams are observed, there are no particles detected in other directions (low fluxes represented by black). On the other hand, the tailwardward streaming particles are accompanied by an isotropic component of low but significant ion fluxes in all directions.

The distribution functions in Figure 3 show examples of the 3D phase space distributions of ion beams projected in the 2D ($v_\parallel$, $v_\perp$) plane. The top panel shows the isocontours of phase space density of an earthward streaming beam (left), counter

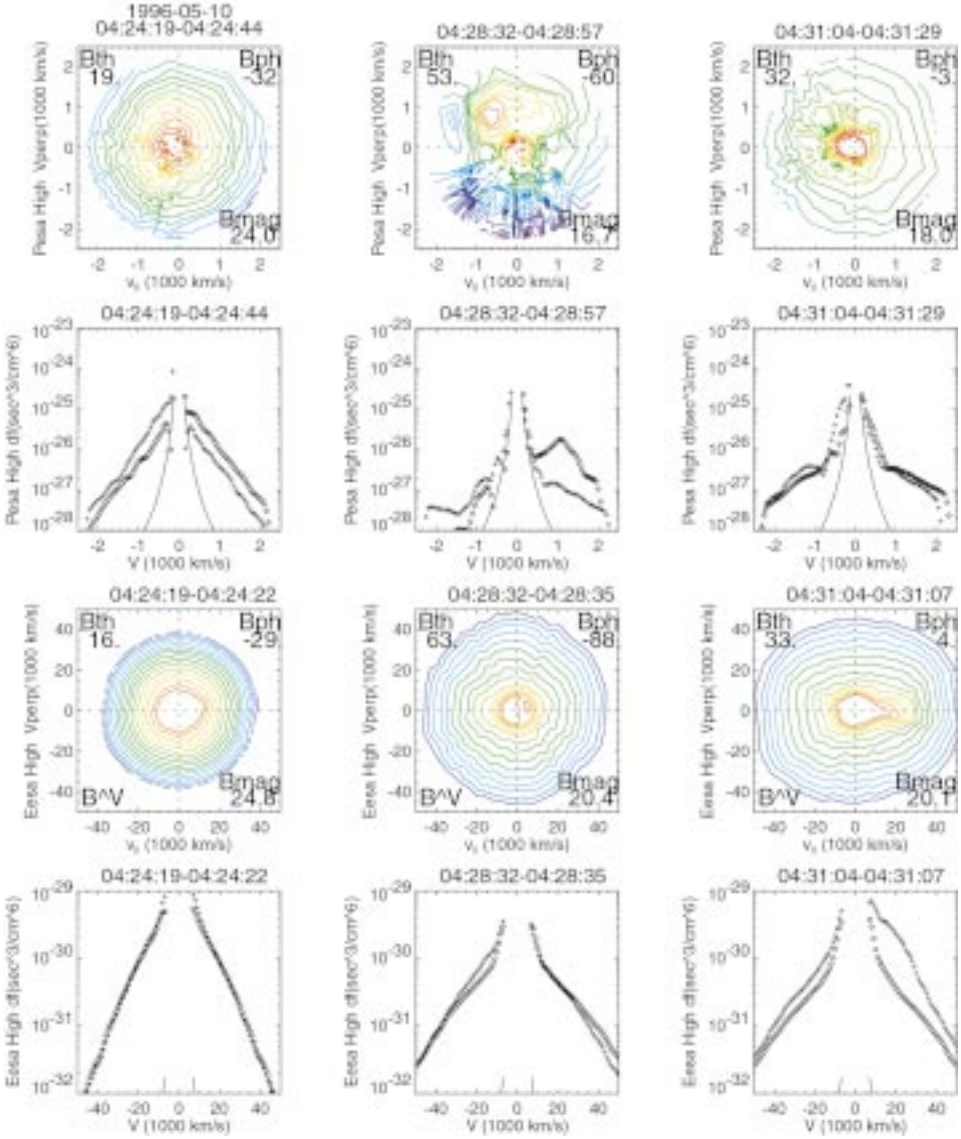

Figure 2. UVI global auroral activities associated with the PSBL observations.

streaming beams (center) and a tailward stream beam (right). Below each contour plot are cuts of the distributions parallel to the direction of **B** (the solid line is instrument one count level). The unidirectional earthward streaming beam seen at 800 km s^{-1} is centered along the magnetic field direction and occupies pitch-angles $\pm 40°$. The width of this beam is 1–2 keV. Corroborating the energy-angle plots, few particles are seen going in the tailward direction (negative half of $v_{\parallel}$ plane). On the other hand, the tailward streaming beam is surrounded by a nearly isotropic

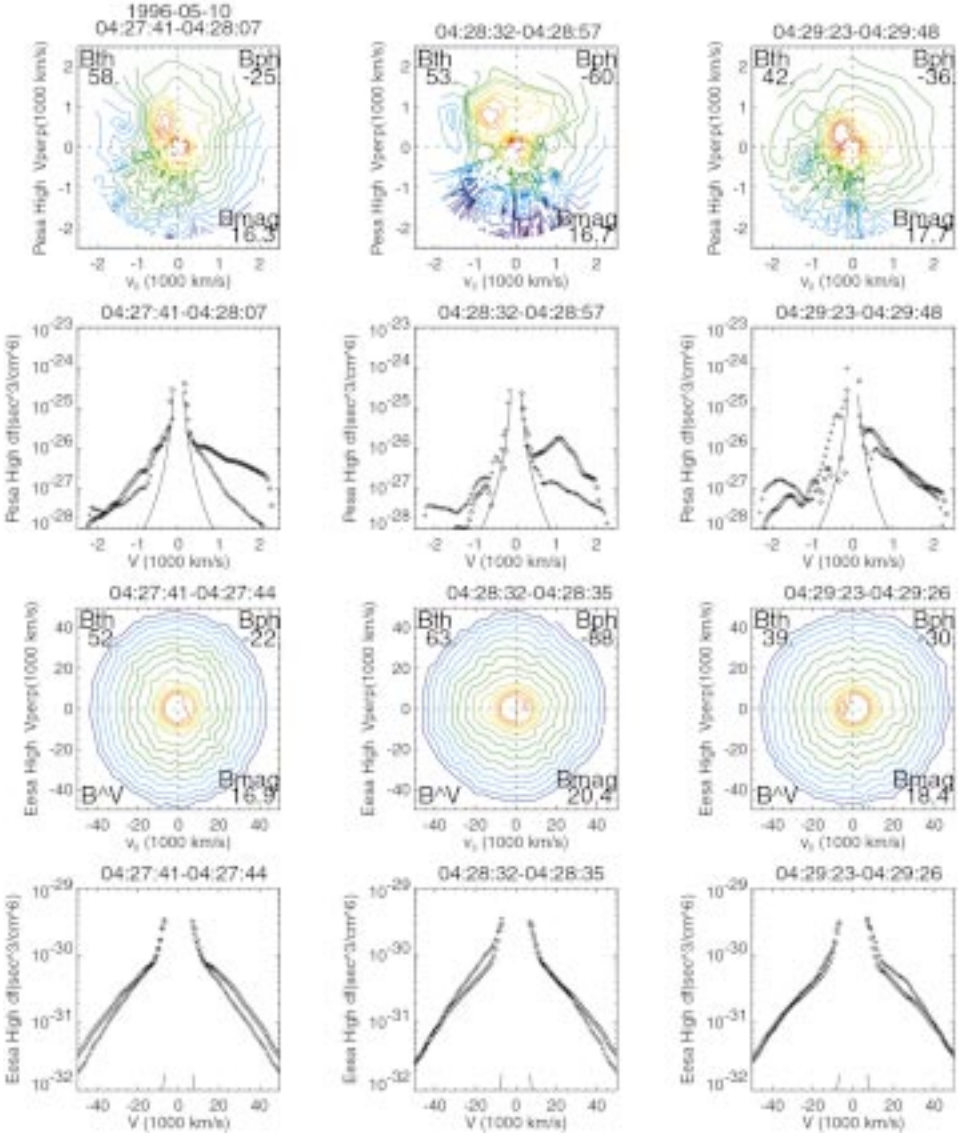

Figure 3. Panels in the first row are isocontours of the ion distribution functions in the $(v_\parallel, v_\perp)$ space. Panels in the second row are cuts of the distribution functions parallel to the direction of the magnetic field.

distribution of higher velocity particles. For the counter streaming case, the beam in the earthward direction at 800 km s^{-1} is more intense but less energetic than the tailward streaming beam at 1000 km s^{-1}. The counter streaming beams also includes isotropic higher velocity particles.

These observations demonstrate that the form of the distribution function affects the outcome of the velocity moments calculation. For example, counter streaming

beams of equal velocity will yield zero mean value. But this does not mean that the plasma is not dynamic. Studying such beams using the velocity moments alone will miss the presence of the beams which provide important information about the plasma dynamics in the PSBL. The large $\langle \mathbf{v} \rangle$ values in the earthward direction results from the distributions where most of the phase space density comes from the beam population. The mixture of a beam and an isotropic distribution yields much smaller $\langle \mathbf{v} \rangle$ values and explains why the mean velocity in the tailward direction in Figure 1 was smaller. Studying the plasma behavior using only moments of the distribution functions can lead to incorrect picture of the actual dynamics.

2.1. New ion beam in the PSBL

Until recently, the outer boundary of the PSBL was reported to consist of only earthward and counter streaming ion beams (Forbes *et al.*, 1982; Takahashi and Hones, 1988). Onsager *et al.* (1991) have modeled the original earthward streaming beam using a steady state neutral line model with convecting magnetic field. This model explains the tailward propagating beam in the counter streaming beams in terms of the reflection of the original earthward streaming beam. New observations (Figures 1 and 3) of unidirectional ion beams propagating in the tailward direction, missed by previous observations, cannot be explained by this model. This beam, which is as intense as the the earthward streaming beam, requires a new theory.

Our observations question the validity of the neutral line model (Onsager *et al.*, 1991). Fuselier and Onsager (1999) challenged our observations. They argued that we were misinterpreting our data and that the instrument was actually observing counter streaming beams. They offered as an explanation that the earthward streaming beam predicted by their model at 300 km s^{-1} that should accompany the tailward streaming beam was not detected because it was masked by our high instrument background. That this is clearly not true and that our instrument is capable of resolving beams at 300 km s^{-1} is discussed in Parks *et al.* (1999).

Our observations indicate that the outer boundary of the PSBL includes a tailward streaming ion beam in addition to earthward and counter streaming beams. The schematic picture given by Takahashi and Hones (1988) of the PSBL must therefore be modified to include this new beam.

2.2. Modulation of PSBL by waves

The PSBL is frequently modulated by large-amplitude waves as evidenced by the alternating pattern of $+\langle vx \rangle$ and $-\langle vx \rangle$ that occurred with a quasi-period of few minutes (Figure 1). This same periodicity is seen in the magnetic field plot. Comparison to Bx shows that $+\langle vx \rangle$ is associated with larger values of Bx and $-\langle vx \rangle$ with smaller values. The density plot shows that $+\langle vx \rangle$ is associated with lower density and $-\langle vx \rangle$ with higher density. If the large Bx and smaller density values mean the spacecraft was closer to the lobe, the $+\langle vx \rangle$ values were observed closer to the lobe and $-\langle vx \rangle$ values further inside the PSBL. Multiple samplings

of the beam reversal region were made as the boundary oscillated back and forth, resulting in the alternating pattern of earthward and tailward streaming beams. This pattern persisted for nearly two hours.

These observations suggest the beams were continuosly present and that the bursty nature of the data are simply due to the spacecraft entering and leaving the beam regions. The fact that ion beams were continuosly observed indicates that the source was also active over the two hour durations. Note that this alternating pattern was interrupted when at 14:10 UT, counterstreaming beams were observed. Comparison to the density plot shows that this occurred in a higher density region. This can be interpreted to mean the counter streaming beams were observed deeper in the PSBL (caution: the time resolution here is 24 s and noting that magnetic field variations are faster, the plasma data could be time aliased).

What is the source of the ion beams in the PSBL and the relationship of the beams to the waves that are modulating the PSBL? These questions are still unanswered. None of the current models include ionospheric sources of beams in the PSBL. Another possible source of the beams comes from acceleration of ions in the current sheet (Speiser, 1965; Zhu and Parks, 1993). The waves might be the same Alfven surface waves with large Poynting fluxes that Polar has observed in association with auroral activity closer to Earth (Wygant *et al.*, 2000).

2.3. Electrostatic waves and spiky electric fields across PSBL

Past observations have established that intense wave activity exists across the narrow region of the outer PSBL where the ion beams are observed (Parks *et al.*, 1984). Two kinds of wave activities are prominant: large amplitude 'spiky' electric field and 'broadband' electrostatic waves (Gurnett *et al.*, 1976). The spiky electric fields have amplitudes as large as 80 mV m^{-1} (Cattell *et al.*, 1982, 1994), which is one to two orders of magnitude larger than the typical convective electric field and can accelerate PSBL particles. The spiky electric fields are associated with lower hybrid waves that may evolve nonlinearly to the spiky structure (Cattell *et al.*, 1984).

The other kind of waves are the broadband electrostatic waves commonly observed in the frequency range from 10 Hz (below the lower hybrid frequency) to the local electron plasma frequency and higher (Gurnett *et al.*, 1976), which now have been shown to consist of groups of nonlinear solitary waves with widths of a few ms (Matsumoto *et al.*, 1994). These nonlinear waves are also observed at auroral altitudes (Ergun *et al.*, 1999), intermediate PSBL region (Cattell *et al.*, 2000) and the bow shock (Matsumoto *et al.*, 1997; Bale *et al.*, 1998).

Before the remarkable discovery of the solitary waves, data suggested that broadband electrostatic waves were driven by ion and electron beams (Parks *et al.*, 1984; Onsager *et al.*, 1993). Recent simulation results show that solitary waves can be produced by electron two streams (Omura *et al.*, 1994). These solitary waves, also known as BGK mode electron phase space holes, have amplitudes typically

a few mV/m but at Polar altitudes they can be as large as 200 mV m^{-1} (Cattell *et al.*, 1999). These nonlinear structures may play a key role in supporting parallel electric fields in the downward current region of the auroral zone, and also in upward current region at Polar altitudes. One important question to be determined is whether the solitary waves observed in the PSBL regions further in the tail also support parallel electric fields. The detailed relationships between the observations of the electrostatic solitary waves and electron and ion beams in the PSBL remain unsolved at this time in part because the time resolutions of existing plasma measurements are not adequate.

3. Dynamics in the Central Plasma Sheet

Away from the PSBL closer toward the CPS and the current sheet (CS) regions, high speed ion flow events are encountered. The most dynamic of these high speed events have velocities >400 km s^{-1} in the earthward direction, called bursty bulk flow (BBF) events (Angelopoulos *et al.*, 1992). The BBFs typically last about 10 minutes and are observed in the CPS region defined by $|B_{xy}| < 15$ nT or $|B_z/B_{xy}| > 0.5$. What do we know about the BBFs besides the high $\langle \mathbf{v} \rangle$ values in the earthward direction? We examine this question with observations made on May 10, 1996 when the Wind spacecraft sampled plasmas from both the PSBL and the CPS regions. The position of the spacecraft at 04 UT was $(-10, 9, 0)$ R_E.

Figure 4 shows a one and a half hour interval of data from the plasma sheet that included BBF events. The top two panels show the ion density and the three components of $\langle \mathbf{v} \rangle$ in the GSE frame. The third panel shows temperatures in different directions where the second moment $\langle v^2 \rangle = \int (v_i - \langle \mathbf{v} \rangle)(v_j - \langle \mathbf{v} \rangle) \mathrm{f}(\mathbf{r}, \mathbf{v}) \mathrm{d}\mathbf{v}$ has been equated to the temperature so that we can compare our observations to work done by others. The fourth panel shows the three components of the magnetic field in GSM. The bottom two panels show spectrograms of particles travelling in the earthward and tailward directions.

3.1. Bursty bulk flow events

The Wind spacecraft until 04:10 UT was in the PSBL region as indicated by large Bx values. Thus the high $\langle \mathbf{v} \rangle$ values observed during this time interval portray the dynamics of the PSBL and are associated with the few keV beams in both directions as can be seen in the spectrograms. The tailward spectrogram also shows a low energy component, from 70 eV (instrument threshold) to 1 keV. The behavior of $\langle \mathbf{v} \rangle$ shows similar patterns as in Figure 1. We see the oscillatory pattern of $+\langle vx \rangle$ and $-\langle vx \rangle$ that are correlated to the denisty variations indicating the PSBL boundary was being modulated. The magnetic field variations are less revealing on this day but Bx shows variations that are roughly correlated with $\langle \mathbf{v} \rangle$.

The spacecraft entered a low density region (lobe) at 04:00 UT in response to a substorm expansion onset at 03:59 UT. The density decreased to 0.01/cc but there

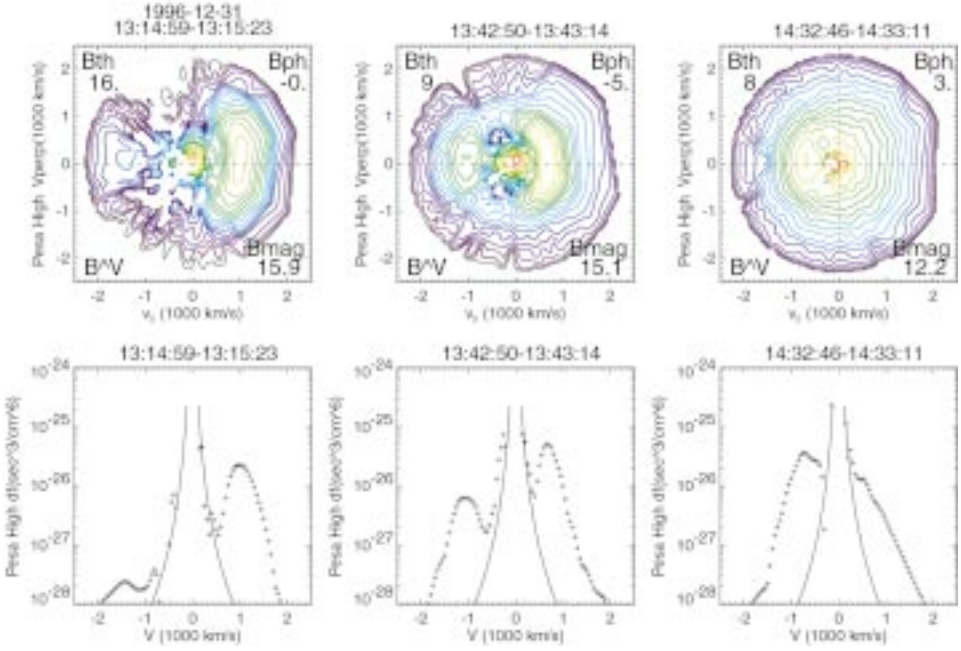

Figure 4. From top to bottom: ion density, ion velocity moments, ion temperatures, magnetic field components, and earthward and tailward travelling ions in spectrogram format.

are two attempts of partial reentry into the PSBL. At 04:10 UT, the spacecraft reentered the PSBL and was accompanied by large variation of the magnetic field, and Bx decreased to values as small as 10 nT. Note also the gradual increase of the temperature starting about the same time. Several bursts of $\langle \mathbf{v} \rangle$ larger than 400 km s^{-1} are subsequently encountered. The event at 04:24 UT is not considered a BBF event because Bx was 30 nT and the spacecraft was sampling the PSBL. But the two bursts between 04:24 and 04:30 UT are BBF events as the spacecraft were in the CPS region. Here, we see $+\langle vx \rangle$ reached 600 km s^{-1} in the earthward direction and complicated high frequency fluctuations accompanied all three magnetic components. This time interval also showed significant values in Vy (400 km s^{-1}) and Vz (-150 km s^{-1}), indicating a pattern much more complex than the earthward flow.

The spectrograms show that the large $\langle vx \rangle$ values of BBFs are associated with the increase of high energy ions up to the highest energy channel of the detector, 28 keV in the earthward direction and decrease of tailward going fluxes (28 keV down to a few keV). BBFs are primarily due to high energy ions. This behavior has been seen in over 50 BBF events we have studied. Following these BBF events, $\langle vx \rangle$ oscillated between positive and negative values and the corresponding increase of ion fluxes associated with them can be seen in the spectrograms. The smaller $\langle \mathbf{v} \rangle$ values are due to the fact the beams are superposed on other isotropic fluxes (more below). Note the appearence of weak fluxes of low energy ions start-

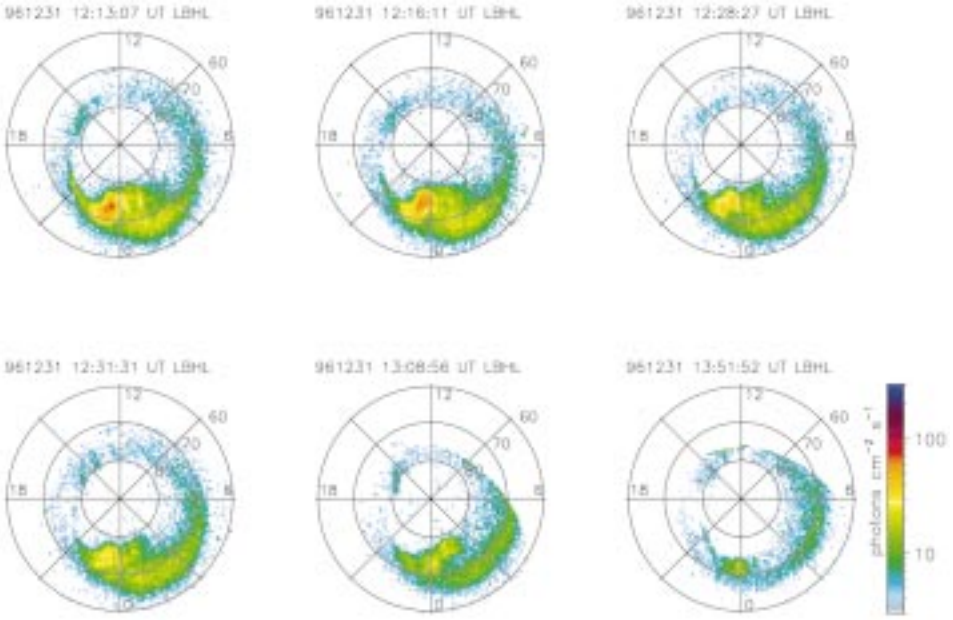

Figure 5. The first and third rows are isocontours of phase space density of ions and electrons in $(v_\parallel, v_\perp)$ space. The second and fourth panels are cuts of the distributions in the directions parallel and perpendicular to the magnetic field.

ing 04:30 UT to past 05 UT. The plasma sheet after BBF events often consist of multicomponent plasmas which can persist for hours (Chen *et al.*, 2000b)

3.2. Distribution function of BBF events

Figure 5 shows examples of three distribution functions of ions and electrons (the electron energy range is similar to the ion range, 100 eV−28 keV) taken before the BBF event (left), during the event (center), and after the event (right). These plots are 25 s averages for ions and 3 s averages of electrons transmitted every 48 s. They are displayed in the spacecraft frame and represent 2D slices (first and third rows) of the 3D distributions along the plane whose normal is defined by $\mathbf{B}x\langle\mathbf{v}\rangle$, where $\langle\mathbf{v}\rangle$ is the mean velocity, with **B** the x-axis and $v_\perp$ the y-axis. Isocontours of the phase space density are shown in $(v_\parallel, v_\perp)$ space. The times are shown on the top and the magnetic elevation (Bth) and the azimuth (Bph) angles are shown on the top right and left. The intensity of the magnetic field is shown on the lower right. The corresponding 1D cuts of the distributions are shown below the contour plots. Both cuts parallel (+) and perpendicular ( ) to the magnetic field direction are show to illustrate the behavior in these principal directions. The solid line represents the instrument background level.

A few minutes before the BBF event, the ion distribution was slightly offset from the origin to the left along the magnetic field direction but was otherwise

symmetric. The offset indicates that more ions were travelling toward the tail. The electron distribution at this time was isotropic although at very low velocities there was a slight hint of anisotropy with the width slightly wider along the magnetic field direction than perpendicular to it.

The ion distribution during the BBF event looks very different. Here we see 'beam-like' feature centered at 50° pitch-angle but extends beyond 90°. In other examples, the beam-like structure is centered about $v_\perp 0$ line (Chen *et al.*, 2000a). There is a sharp 'boundary' at 1000 km s^{-1} in the direction parallel to B and most of the phase space density populates the upper half of the $v_\perp$ plane. The 1D cuts illuminate the complex phase space structures in the two principal directions and show clearly that the plasma population includes more than one component. The velocity moments shown in Figure 4 are computed from convolving this kind of complex distribution.

The contours of high velocity electrons are nearly isotropic and they become anisotropic at lower velocities with the width wider in the parallel direction over the perpendicular direction by about 20%. The electrons include two different populations and note also the origin is offset to the left indicating more electrons are travelling toward the tail direction.

The column on the right shows the phase space features after the BBF event. Here the contours at high velocities appear to be recovering toward isotropy but we now see that there are more high velocity particles. This is indicated by the wider spacings of the contours and more clearly shown in the 1D cut along the magnetic field direction. There is now also a core of low velocity ions with slight offset of the the origin toward the negative $v_\parallel$ direction, indicating more ions are travelling toward the tail direction. The electron distributions now show large anisotropy for all velocities and includes a narrow beam travelling along B in the earthward direction. This beam comes from electrons with energies less than about a keV and occupies $\pm 10°$ pitch-angle range which is the instrument angular resolution. The details about these electron beams are discussed in Chen *et al.* (2000). This is another case that illustrates that the particle population in the CPS region consists of multicomponent plasmas (Chen *et al.*, 2000b).

Figure 6 shows a sequence of three successive distributions taken during the BBF event to illustrate their temporal development. The format of these plots is the same as in Figure 5 and the middle column is a repeat of the BBF distribution shown in that figure. These plots indicate that both ion and electron distributions during BBFs are evolving in time in a complex way. There is no obvious indication that the BBFs are being transported by an $\mathbf{E} \times \mathbf{B}$ drift. We indicated earlier with Figure 4 that the magnetic field fluctuated considerably during the BBF event. These fluctuations occur much faster than the sampling time of the distribution function, and the reader is cautioned that the ion distributions obtained with 25 s time resolution will be time aliased if there were faster time variations occurring. Thus, 25 s distributions we show must be viewed as 'smeared out' picture. The

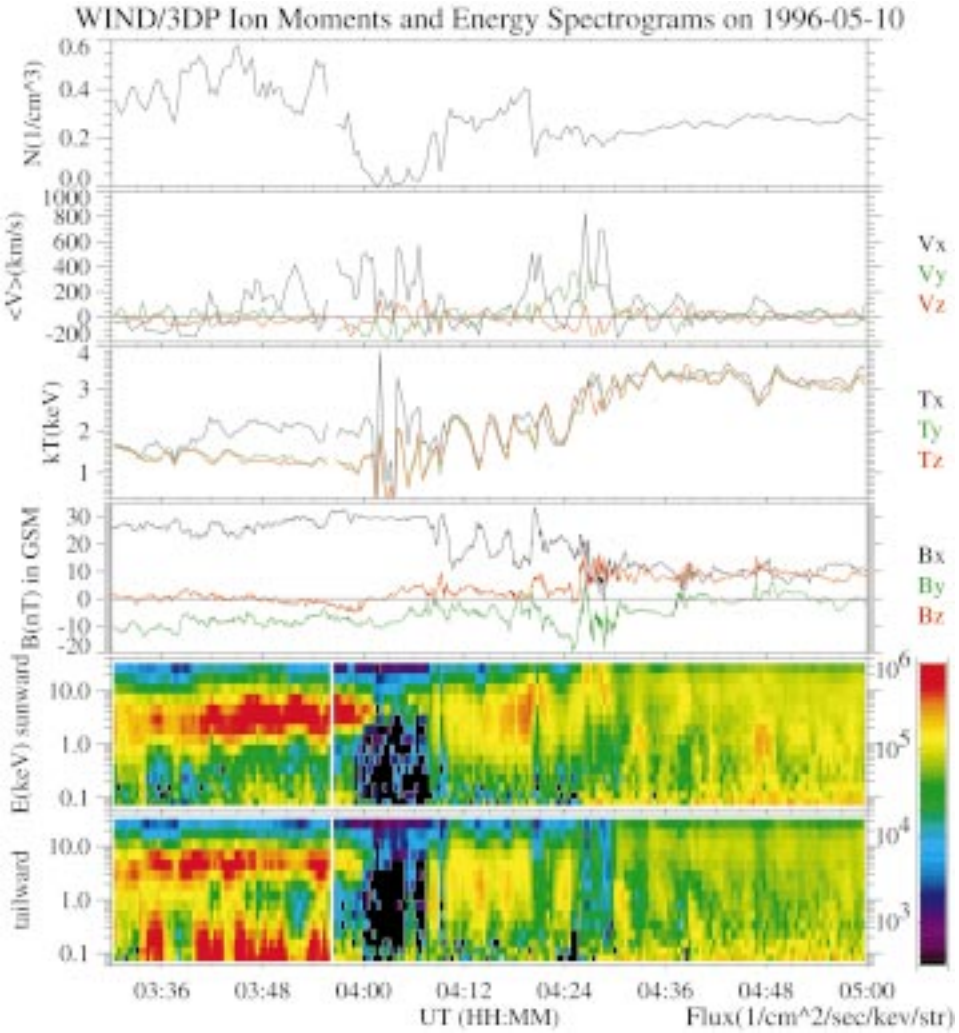

Figure 6. Format is same as in Figure 5. Subsequent distributions to show the evolutionary and dynamic nature of the BBF event.

sequence in Figure 6 however demonstrates that the ion dynamics is very complex during a BBF event.

The electron distributions also show their dynamics can be quite complex. The electron anisotropy changes during the event. Early on at the beginning of the event, the anisotropy indicated ‘trapped-like’ distribution with more electrons in the perpendicular direction. But this anisotropy changed as the next two distributions show larger anisitropy in the parallel direction. The offsets also changed from left to right as can be seen from the 1D cuts in the second and third columns.

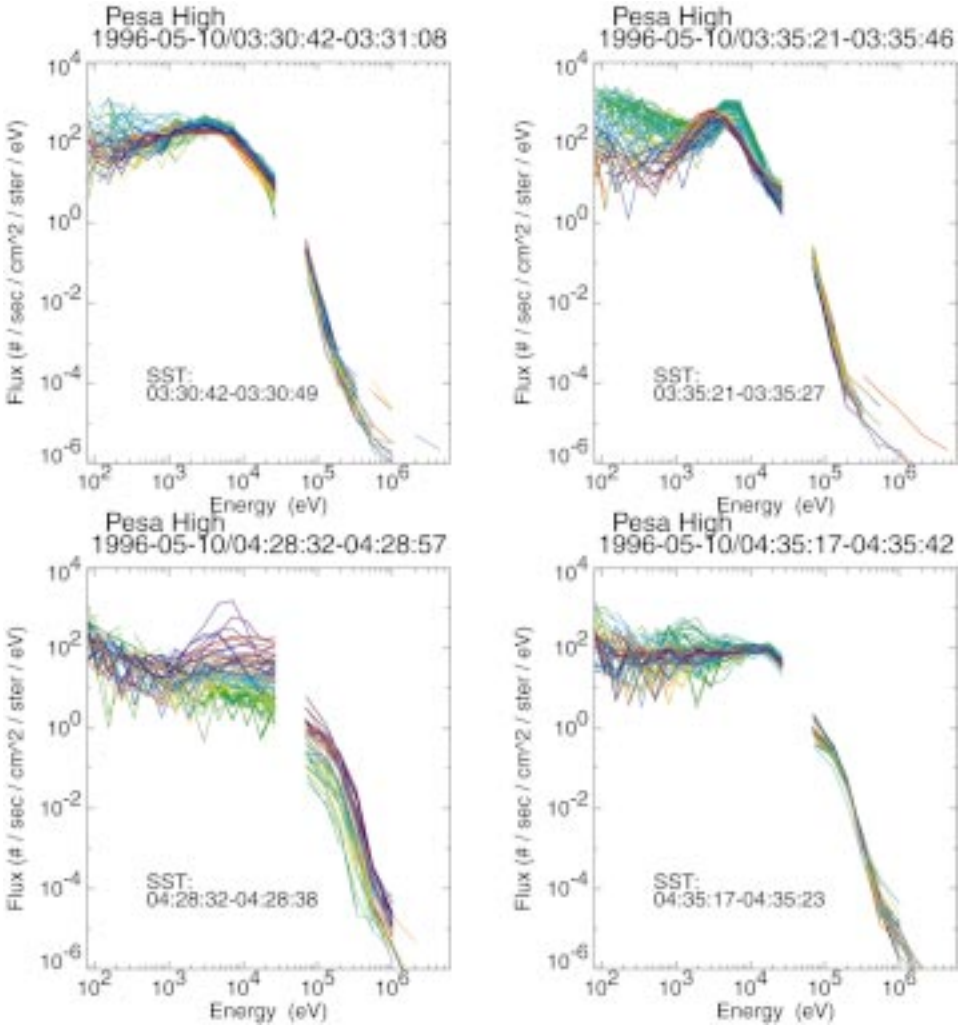

Figure 7. Energy spectra from 70 eV to several MeV to illustrate the anisotropic nature of the BBF ions.

3.3. Acceleration of ions to MeV energies during BBF events

We indicated in connection with Figure 4 that a significant increase of energetic ions is associated with the BBF events. Figure 7 shows plots of ion energy spectra from 70 eV to several MeV obtained by the electrostatic analyzers (ESA) and the solid state telescopes (SST). Energy spectra from 120 angular bins are displayed for the ESA and 44 for the SSTs to reveal the directional information about the ion fluxes. SST data are 6vs averages transmitted every 48 s. The red, purple, and black are particles travelling toward the Earth and the green toward the tail. For purposes of comparison, we show energy spectra from both the PSBL and CPS.

The energy spectra shown on the top left were obtained at 0331 when the spacecraft was in the PSBL. The spectra on the top right also comes from the PSBL region but at this time one can see the presence of counter streaming beams. Note that the beam energy travelling in the tailward direction (green) is more energetic than the beam travelling in the earthward direction. Both of the spectra show very little spread of the various spectral lines, indicating that the fluxes are fairly isotropic (except at very low energies).

The spectra shown on the bottom left were obtained at 04:29 UT during the BBF event discussed above. This figure indicates energetic ions to MeV energies accompany BBF events and that more fluxes are detected travelling in the earthward direction for energies larger than 1 keV. The spreading of the various spectral lines indicates that a considerable amount of directional anisotropy exists for ions up to MeV energies. The spectra during the BBF event is complicated and does not represent a simple Galilean shift of the pre-BBF spectrum. The indications are that time dependent and nonadiabatic effects are present.

The energy spectra on the bottom right panel is taken at 04:35 UT after the BBF event. Here we see that the spectra are nearly isotropic, but note the larger intensities of the higher energy particles. We have only discussed here ion acceleration. Electrons are also accelerated to hudreds of kev during BBF events (not shown).

3.4. BBFs, UV EMISSIONS, AND AURORAL KILOMETRIC RADIATION

Angelopoulos *et al.* (1997) and Fairfield *et al.* (1999) indicated that BBFs in the CPS occur with the substorm expansion phase. We have studied neary 50 BBF events and find that BBFs can occur at any time during the substorm and not confined just to the onset. BBFs even occur with very weak auroral activities. Fairfield *et al.* (1999) further note that these substorm onset associated BBFs are accompanied by the AKR activity. We show below that this correlation exists not just at the expansion onsets but they exist for all BBF events we have studied.

On July 26, 1997 a series of more than 10 high speed flow events was detected during a three hour period when Wind was in the vicinity of the CPS region. The top panel of Figure 8 shows the key parameters (3-min time resolution) AKR data (courtesy of M. Kaiser and J. L. Bougeret) plotted to the same time scale as the keogram of UVI auroral images taken near local midnight. The panel below it shows the energy flux deposited by electron precipitation, estimated from the UVI images. On the basis of the amount of energy deposited during these events and that none of the auroral brightening expanded in the classical sense of the auroral substorm (Akasofu, 1966), we have concluded the auroral brightenings are due to ‘pseudobreakup’ events. The four global images from a selected interval are shown on top to illustrate the weak nature of the auroral activity associated with two of the pseudobreakup events. The solar wind during this interval was fairly quiet and the IMF Bz was predominantly in the northward direction (2 nT). (We realize that

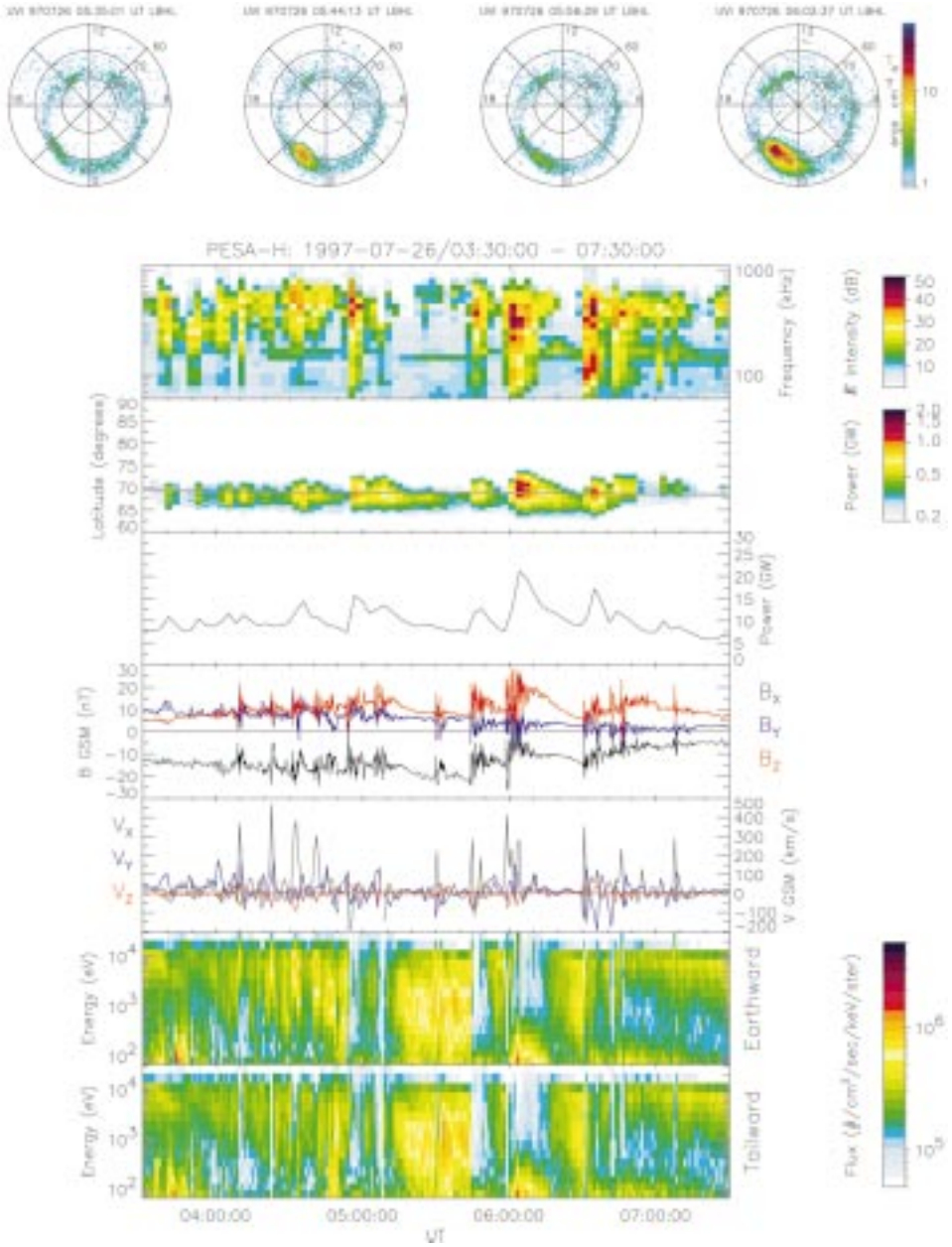

Figure 8. From top to bottom: Examples to illustrate the pseudobreakup auroral events from the UVI camera, AKR emissions, keogram of the aurora, energy deposited in aurora, three components of the magnetic field, three velocity moments, and energy spectrograms of earthward and tailward travelling ions.

one could argue that each of the pseudobreakup events is actually a substorm and that the criterion is rather subjective.)

The fourth panel shows the velocity moments $\langle \mathbf{v} \rangle$ of ions. The panels below show the spectrograms of ions travelling earthward and tailward and the panel just above show the three components of the magnetic field measured by Wind. A number of these high $\langle \mathbf{v} \rangle$ events have earthward directed speeds >400 km s^{-1} and they are accompanied by Bz increases and high frequency magnetic fluctuations. We thus classify them as BBF events. Note that while the magnetic field showed increases of the Bz component, they are not the 'usual' dipolarizations since they are accompanied by high frequency oscillations.

Comparison of these pseudo auroral breakup activities to the plasma $\langle \mathbf{v} \rangle$ data indicates that each increase of auroral brightening and intensification of the AKR emission is associated with increases of $\langle \mathbf{v} \rangle$ but the reverse is not true. What is remarkable about this observation is that high speed flow events can be observed in the CPS region with relatively weak solar wind and auroral activites. The large high speed $\langle \mathbf{v} \rangle$ events (06 UT, for example) are accompanied by acceleration of ions to MeV energies (not shown).

4. Summary and Conclusion

We have discussed in this article several new observations about the behavior of plasma behavior in the PSBL and the CPS region. We have shown that (1) unidirectional ion beams propagate in the tailward direction in the outer PSBL boundary, (2) plasma distributions in the PSBL where earthward and tailward streaming ions are observed are quite different and studying velocity moments alone is inadequate, (3) PSBL is continually modulated by waves, (4) the high velocity moments of BBFs in the CPS regions are mainly due to anisotropic high energy ions, (5) BBFs coicide with high frequency magnetic fluctuations that are comparable to ion cyclotron period, (6) BBFs occur at various levels of auroral activities, (7) ions are accelerated to MeV energies during BBFs, and (8) after BBF events, the distribution in the CPS region consists of multicomponent plasma that persists for hours.

The modulated pattern of $\langle \mathbf{v} \rangle$ across the PSBL boundary suggests that the beams are there for a long time. We inferred from previous observations that the beams occupy the same region where large spiky electric fields and electrostatic solitary waves are observed. The current theory is that the spiky electric fields are nonlinear development of lower hybrid waves and the solitary waves are nonlinear development of electrostatic waves produced in two stream instability. Previous observations gave some indications about their presence but the observations are not conclusive and requires further studies (Parks *et al.*, 1984; Onsager *et al.*, 1993).

The BBFs in the CPS region show complex distributions and they are observed to occur throughout a substorm disturbance. They are correlated with increases of

Bz and high frequency magnetic field fluctuations, strongly suggesting that BBFs are associated with the disruption of the tail current. Although the mechanism for the disruption is not yet identified, we note that the magnetic field fluctuations are often near the frequency of proton cyclotron period. Similar kind of magnetic fluctuations have been made by Lui *et al.* (1992) and near synchronous altitudes they have been identified as ion cyclotron waves (Perraut *et al.*, 2000). The generation mechanism of BBFs is quite dynamic as ions are accelerated to MeV energies and electrons to hundreds of keV. The BBF distributions yield large $\langle \mathbf{v} \rangle$ because the distributions are highly anisotropic. The large $\langle \mathbf{v} \rangle$ is not due to $\mathbf{E} \times \mathbf{B}$ flows. This activity is not confined to just in the CPS region as both AKR and auroral brightening occur during the BBF events. The generating mechanism affects both 'global' currents in the CPS and smaller scale microphysical processes that produce unstable electron distribution and precipitation to excite auroral and AKR emissions at lower altitudes.

Future observations must address how the microphysical process that are active in the plasma sheet regulate the transfer of mass, momentum and energy into the aurora. This is a challenge to long-standing unsolved problem of great importance to space physics. We hope the new observations presented in this article will inspire and initiate work on new kinetic models and theories that will properly describe fundamental collisionless plasma processes.

Acknowledgement

The research work at the University of Washington is supported by NASA grants NAG5-3170 and NAG5-7714.

References

Angelopoulos, V., Baumjohann, W., Kennel, C., Coroniti, F., Kivelson, M., Pellat, R., Walker, R., Luhr, H. and Paschmann, G.: 1992, *J. Geophys. Res.* **97**, 4027.

Angelopoulos, V., Phan, T., Larsen, D., Mozer, F., Lin, R., Tsuruda, K., Hayakawa, H., Mukai, T., Kokubun, S., Yamamoto, T., Williams, D., McEntire, R., Lepping, R., Parks, G., Brittnacher, M., Germany, G., Spann, J., Singer, H. and Yumoto, K.: 1997, *Geophys. Res. Lett.* **24**, 2271.

Bale, S., Kellogg, P., Larsen, D., Lin, R., Goetz, K. and Lepping, R.: 1998, *Geophys. Res. Lett.* **25**, 2929.

Baumjohann, W., Paschmann, G. and Luhr, H.: 1990, *J. Geophys. Res.* **95**.

Cattell, C., Kim, M., Lin, R. P. and Mozer, F.: 1982, *Geophys. Res. Lett.* **9**, 539.

Cattell, C., Mozer, F., Tsuruda, K., Hayakawa, H., Nakamura, M., Okada, T., Kokubun, S. and Yamamoto, T.: 1994, *Geophys. Res. Lett.* **21**, 2987.

Cattell, C., Bergmann, R., Hudson, M., Kletzing, C., Mozer, F., Temerin, M., Roth, I. and Parks, G.: 2000, 'Comparison of Solitar Waves and Wave Packets Observed at Plasma Sheet Boundary to Observations in the Auroral Zone', *Alfvén Conference Proceedings*, to be published.

Chen, L. J., Larson, D., Lin, R., McCarthy, M. and Parks, G. K.: 2000a, *Geophys. Res. Lett.*, submitted.

Chen, L. J., Larson, D., Lin, R., McCarthy, M. and Parks, G. K.: 2000b, *Geophys. Res. Lett.* **27**, 843.
Ergun, R., Carlson, C., McFadden, J., Mozer, F., Delory, G., Peria, W., Chaston, C., Temerin, M., Roth, I., Muschietti, L., Elphic, R., Strangeway, R., Pfaff, R., Cattell, C., Klumpar, D., Shelley, E., Peterson, W., Mobius, E., and Kistler, L.: 1998, *Geophys. Res. Lett.* **25**, 2041.
Fairfield, D., Mukai, T., Brittnacher, M., Reeves, G., Kokubun, S., Parks, G., Nagai, T., Matsumoto, H., Hashimoto, K., Gurnett, D. and Yamamoto, T.: 2000, *J. Geophys. Res* . **104**, 355.
Fillingim, M., Parks, G. K., Chen, L. J., Brittnacher, M., Germany, G., Spann, J., Larson, D. and Lin, R.: 2000, *Geophys. Res. Lett.*, to be published.
Forbes, T., Hones, E. W., Bame, S., Asbridge, J., Paschmann, G., Sckopke, N. and Russell, C.: 1982, *Geophys. Res. Lett.* **8**, 261.
Fuselier, and Onsager, T.: 1999, *Geophys. Res. Lett.* **26**, 2935.
Gurnett, D., Frank, L. and Lepping, R.: 1976, *J. Geophys. Res.* **81**, 6059.
Lin, R. P., Anderson, K., Ashford, S., Carlson, C., Curtis, D., Ergun, R., Larson, D., Mcfadden, J., McCarthy, M., Parks, G., Reme, H., Bosqued, J., Coutelier, J., Cotin, F., d'Uston, C., Wenzel, P., Sanderson, T., Henrion, J., Ronnet, J. and Paschmann, G.: 1995, *Space Sci. Rev.* **71**, 125.
Lui, A. T. Y., Lopez, R., Anderson, B., Takahashi, K., Zanetti, L., McEntire, R., Potemra, T., Klumpar, D., Greene, E. and Strangeway, R.: 1992, *J. Geophys. Res.* **97**, 1461.
Matsumoto, H., Kojima, H., Miyatake, T., Omura, Y., Okada, M., Nagano, I. and Tsutsui, M.: 1994, *Geophys. Res. Lett.* **21**, 2915.
Matsumoto, H.: 1997, *Adv. Space Res.* **20**, 683.
Omura, Y., Kojima, H. and Matsumoto, H.: 1994, *J. Geophys. Res.* **101**, 2685.
Onsager, T., Thomsen, M., Elphic, R. and Gosling, J.: 1991, *J. Geophys. Res.* **96**, 20999.
Onsager, T., Thomsen, M., Elphic, R., Gosling, J., Anderson, R. and Kettmann, G.: 1993, *J. Geophys. Res.* **98**, 15509.
Parks, G. K., McCarthy, M., Fitzenreiter, R., Etcheto, J., Anderson, K., Anderson, R., Eastman, T., Frank, L., Gurnett., D., Huang, C., Lin, R., Lui, A. T. Y., Ogilvie, K., Pedersen, A., Reme, H. and Williams, D.: 1984, *J. Geophys. Res.* **89**, 8885.
Parks, G. K., Fitzenreiter, R., Ogilvie, K., Huang, C., Anderson, K., Dandouras, J., Frank, L., Lin, R., McCarthy, M., Reme, H., Sauvaud, J. and Werden, S.: 1992, *J. Geophys. Res.* **97**, 2943.
Parks, G. K., Chen, L. J., McCarthy, M., Larson, D., Lin, R., Phan, T., Reme, H. and Sanderson, T.: 1998, *Geophys. Res. Lett.* **25**, 3285.
Parks, G. K., Chen, L. J., McCarthy, M., Larson, D., Lin, R., Phan, T., Reme, H. and Sanderson, T: 1999, *Geophys. Res. Lett.* **26**, 2639.
Perraut, S., *et al*.: 2000, Current driven electromagnetic ion cyclotron instability at substorm onset, *J. Geophys. Res.*, submitted.
Speiser, T.: 1965, *J Geophys. Res.* **70**, 4219.
Takahashi, K. and Hones, E., Jr.: 1988, *J. Geophys. Res* **93**, 8558.
Wygant, J., Keiling, A., Cattell, C., Johnson, M., Temerin, M., Mozer, F., Kletzing, C., Scudder, J., Peterson, W., Russell, C., Parks, G. and Brittnacher, M.: 2000 *J. Geopys. Res.*, submitted.
Zhu, Z. and Parks, G. K.: 1993, *J. Geophys. Res.* **98**, 7603.